Realistic Metal–Graphene Contact Structures

Cheng Gong, Stephen McDonnell, Xiaoye Qin, Angelica Azcatl, Hong Dong, Yves J. Chabal, Kyeongjae Cho,* and Robert M. Wallace*

Department of Materials Science and Engineering, The University of Texas at Dallas, Richardson, Texas 75080, United States

ABSTRACT The contact resistance of metal–graphene junctions has been actively explored and exhibited inconsistencies in reported values. The interpretation of these electrical data has been based exclusively on a *side*-contact model, that is, metal slabs sitting on a pristine graphene sheet. Using *in situ* X-ray photoelectron spectroscopy to study the wetting of metals on as-synthesized graphene on copper foil, we show that side-contact is sometimes a misleading picture. For instance, metals like Pd and Ti readily react with graphitic carbons, resulting in Pd- and Ti-carbides. Carbide formation is associated with C–C bond breaking in graphene, leading to an *end*-contact geometry between the metals and the periphery of the remaining graphene patches. This work validates the *spontaneous* formation of the metal–graphene end-contact during the metal deposition process as a result of the metal–graphene reaction instead of a simple carbon diffusion process.

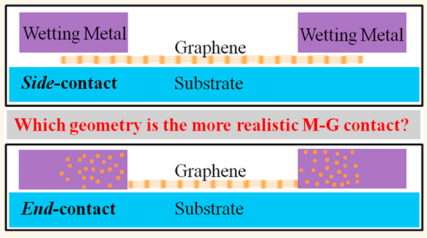

KEYWORDS: graphene · metal · interface reaction · carbide · end-contact · X-ray photoelectron spectroscopy

The contact resistance for metals to graphene continues to be a key limitation in device applications. The low-field electrical transport behavior of graphene, characterized by the conductivity (σ) as a function of gate voltage (V_g), shows a characteristic "V shape" with the conductivity minimum indicating the position of the Dirac point of the graphene channel.[1] Metal electrodes (*e.g.*, Pt or Au) that weakly interact with graphene, without chemical bond formation or substantial interface hybridization, preserve the graphene linear π-band dispersion[2−5] and dope graphene in the contact regions, leading to n-i-n or p-i-p junction formation throughout the device.[6,7] The conductivities of such junctions are expected to have "W shape" with two minima as a function of V_g at the Dirac points of the doped and intrinsic graphene.[6,7] This type of contact geometry is termed "side-contact",[8−10] often assumed to be metal slabs on the pristine graphene. The junction model, albeit successful for understanding the electronic transport through the graphene side-contacted by weakly interacting metals, fails to interpret more realistic interfaces with widely used "wetting" electrodes (viz., Pd,[11,12] Ti,[13,14] Cr,[15] Ni,[16] and Co[15]). In fact, the weakly interacting metal–graphene interfaces pose a practical adhesion problem causing electronic devices to fail through delamination. This is a primary reason that wetting metals with strong interfacial interaction are favored in graphene nanoelectronics.

Nearly all the analysis of the electrical data from the wetting metal–graphene contact has been performed based on the side-contact model,[12,17,18] which deserves careful scrutiny. Essentially, the wetting electrodes may affect not only the electronic (*i.e.*, disturbing the π-electron linear dispersion by metal d- and carbon π-orbital hybridization) but also the structural properties of graphene (*e.g.*, forming a carbide,[19] probably initiated by transition metal adatoms reacting with defect regions[20]). Without careful structural characterization, it is therefore risky to assume that graphene remains intact while in contact with such reactive metals. For example, early in carbon nanotube (CNT) research, the Ti-CNT end-contact geometry was proven to be preferable at $T > 800$ °C by Zhang *et al.*[21] as a result of the formation of a carbide layer at the contact, followed by the theoretical investigation by Léonard and Tersoff.[22] Particularly, it is important to note that the electron-beam deposition process, under carefully controlled ambient conditions, contains a number of reactive metal atoms and nanoclusters that readily disrupt the planar sp^2-bonded network

* Address correspondence to rmwallace@utdallas.edu, kjcho@utdallas.edu.

Received for review October 8, 2013 and accepted November 21, 2013.

Published online November 21, 2013
10.1021/nn405249n

of graphene.[23] Lahiri *et al.* experimentally demonstrated the easy formation of nickel carbide at 100 °C when Ni is deposited on the as-synthesized graphene, in sharp contrast to graphene on Ni substrate that can be stable up to 650 °C.[19] Lahiri *et al.*'s work highlighted the notable difference between graphene interfacing with metal substrate and with deposited metals. However, intensive efforts have been mostly focused on characterizing the epitaxial graphene on metal templates rather than the graphene covered by deposited metal layers, even though they can form quite different interface structures. At the former interface, graphene is formed on a metal surface with more commensurate morphology, but the latter interface formation process is more reactive due to the chemically aggressive metal atoms and clusters deposited on graphene. Electrical characterization, although being widely performed in numerous devices,[11−18,24] cannot provide interfacial chemical bonding information. Therefore, it is important to determine the interfacial chemistry between graphene and deposited wetting metals in order to elucidate contact issues.

Titanium and palladium are the two representative wetting metals studied in this work. First, Pd differs from other more reactive metals (*i.e.*, Ti, Ni, Cr, and Co) which favor oxidization or carbidization.[25,26] Remarkably, experimental observations reveal that Pd electrodes have a lower contact resistance than Ti electrodes when contacting graphene.[27] In contrast, most transport simulations conclude that Ti is a superior contact over Pd.[28−30] Palladium in contact with metallic CNTs (m-CNTs) was claimed to achieve more reliable performance (*i.e.*, reproducibility) than Ti, which was ascribed to the possible oxidation of Ti in the vacuum environment employed.[31] Second, although Pd has a similar electronic configuration to Pt, these metals behave differently in both graphene and CNT electronics.[32] Palladium, with a lower work function, was shown to form a p-type Ohmic contact where Pt, with a higher work function, otherwise formed a non-Ohmic contact with m-CNTs.[31,33] Javey *et al.* attributed this unexpected result to the more favorable interaction between Pd (than Pt) and the CNT sidewall.[33] The mechanism of how the favorable metal interaction promotes the electrical performance of graphene electronics remains elusive. Xia *et al.*'s work[12] highlighted the important contribution of the charge transport through the graphene underneath Pd contact, whereas Mann *et al.*[31] emphasized that the charge injection mainly occurs at the edge of Pd contact to the CNT. To provide insights for a better understanding of these issues, we chose Pd and Ti for this study.

RESULTS AND DISCUSSION

We deposited Pd and Ti separately on as-grown graphene on copper foil at room temperature under ultrahigh vacuum (UHV) conditions, followed by an *in situ* X-ray photoelectron spectroscopy (XPS) study of the interfacial bonding chemistry. In order to probe the real interaction between deposited metals and graphene, three precautions were taken. (i) The deposition chamber ambient condition must be under very low pressures ($\sim 10^{-9}$ mbar) to avoid spurious oxidation and/or catalyzed carbidization with residual water typically present in elastomer-sealed evaporators, particularly for Ti deposition;[34,35] (ii) the graphene samples must be clean, free of carbon or oxygen contamination;[36,37] (iii) the metal deposition and XPS characterization processes must be done without vacuum interruption to avoid or minimize spurious oxidation/contamination. The concurrent fulfillment of all three precautions rules out the impact of oxygen- and carbon-bearing contaminants, from either the deposition chamber[26] or the graphene surface.[38] Therefore, in the series of experiments reported here, a clustered UHV system[39] is utilized to provide the following conditions: (i) $\leq 10^{-9}$ mbar is maintained in the UHV cluster, including the deposition chamber ($\sim 1 \times 10^{-9}$ mbar), XPS chamber ($\sim 3 \times 10^{-10}$ mbar), and the transfer tube ($\sim 2 \times 10^{-11}$ mbar) connecting the two chambers; and (ii) as-grown graphene on a copper foil[27] is used instead of the polymer-aided transferred graphene on SiO_2 where residues are evident.[36,40] Only through the careful control of these conditions can XPS data be reliably translated into an understanding of the metal−graphene interaction.

Possible Metal−Graphene Interface Configurations. Before the detailed discussion of the experimental results, four types of metal−graphene interface bonding configurations are first illustrated in Figure 1b−e. Note that the morphology of metal adsorptions[41] on graphene is not the focus of this study, while the chemical reaction and the corresponding metal−carbide alloy formation are emphasized. Angle-resolved XPS (ARXPS, see Figure 1a) data are employed to identify which configuration represents the actual interface.

Titanium−Carbide Formation. Figure 2a,b shows the progression of both the Ti 2p and the C 1s core levels with the deposition of titanium on graphene synthesized on a copper foil. The raw Ti 2p spectra show the increase in the titanium surface concentration with each deposition stage. The C 1s spectra have been normalized so that the changes in the bonding environments can be tracked more clearly. The initial spectrum consists of a single asymmetric feature with a peak maximum at 284.6 eV (typical of graphite[42] and consistent with graphene[36,37]). After the first deposition of titanium, there is the appearance of a new asymmetric feature at 281.8 eV, which is close to the reported value of 281.7 eV for titanium carbide.[42] The appearance of the carbide feature is concurrent with the decrease in the graphene C 1s feature, suggesting that titanium is reacting with the graphene to form carbide. As the deposition continues, the intensity ratio of carbide to graphene continually increases. Meanwhile, a 0.3 eV upward shift of the C 1s binding energy

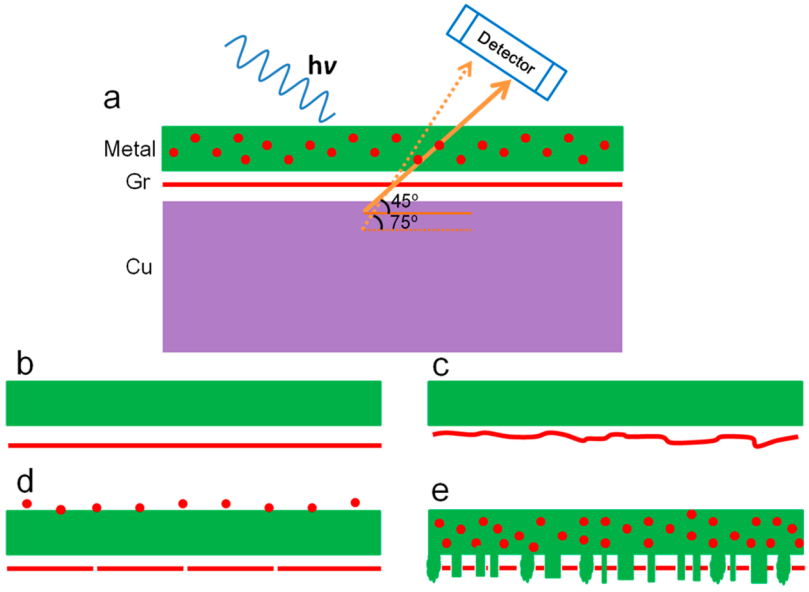

Figure 1. (a) Illustration of the ARXPS measurement of the metal−Gr/Cu sample. (b−e) Illustration of the four possible metal−graphene interface scenarios. Due to the photoelectron escape depth, a 45° takeoff angle measurement is more surface sensitive, whereas the 75° measurement probes more of the bulk. For the interface scenario (b), graphene remains highly pristine upon metal deposition on top and is analogous to the side-contact scenario. For the interface scenario (c), graphene maintains its structural integrity, but the flatness is somewhat distorted. For interface scenario (d), a tiny amount of carbon atoms are extracted and diffuse through the metal layers and onto the metal surfaces, due to the very limited carbon solubility in the metal. For interface scenario (e), strong chemical reaction occurs between the deposited metal and graphene, and the graphene is thereby consumed, resulting in carbide formation and a metal−graphene end-contact. Figures are not to scale.

after 105 min deposition is caused by the n-type doping of graphene by the low work function Ti contacts.[24] The conversion from graphene to carbidic bonding with the deposition of titanium suggests that the underlying graphene reacts with the deposited Ti, forming a Ti−C alloy.

This carbide formation indicates an end-contact between titanium and the remaining nonreacted graphene (illustrated in Figure 2f). Carbide formation, as a carbon−metal alloy, is an unambiguous indication of the fact that carbon atoms belonging to the graphene lattice are partially or completely dissolved into the bulk metal. Upon the destruction of the graphene lattice, the metal spontaneously bonds to the edge of the remaining nonreacted graphene sheet, resulting in an end-contact. It is important to note that the observed carbide peak corresponds to the alloy but is not a direct sample of the relatively small population of metal−carbon bonding at the graphene edges, which is expected to be below the limit of detection.

Palladium−Carbide Formation. Compared to the high chemical reactivity of Ti, the Pd reaction with graphene is subtle and requires more careful examination. The signatures of Pd−carbide bonding are found in the C 1s and Pd $3d_{5/2}$ core level shifts in the XPS spectra of both Pd−graphene/Cu and Pd−HOPG contacts.

Figure 2c shows the Pd−carbide formation upon a deposition of ∼0.6 nm Pd on as-grown graphene on a copper foil. The Pd 3d peak is deconvoluted into two peaks: one is the metallic Pd reference peak, and the other is located at a 0.6 eV higher binding energy. Pd−carbide has been observed to be typically 0.6 eV higher than the metallic Pd 3d core level.[43−45] Considering the minimal detection of remnant oxygen at the Cu−graphene interface by XPS and to ensure that the 0.6 eV higher Pd 3d component (shaded zone in Figure 2c) is not caused by Pd−O bonding, a comparative experiment is done on an oxygen-free HOPG sample (see Figure S1 and the related text in the Supporting Information). In Figure 2c, the same 0.6 eV higher component in the Pd 3d peak is observed in a Pd−HOPG contact, substantiating the assignment of this peak to Pd−carbide. According to the ratio between Pd−carbide and the metallic Pd peak intensity, the Pd−C atomic ratio in the alloy is estimated to be ∼5.5:1, which is close to the other reported value of 6:1,[43] far exceeding the room temperature carbon solubility (<0.1%) in Pd.[46]

Now we turn our attention to the Pd−carbide C 1s peak. Due to the large population of carbon in graphene, the newly formed carbide signal is difficult to resolve. Furthermore, the literature shows that the Pd−carbide feature for C 1s (284.3 eV[47] and 284.1 eV[48]) is slightly below the normal binding energy of sp^2-C in graphene. Both reasons make the recognition of the Pd−carbide feature within the C 1s envelope challenging. In order to establish the carbide chemical shift, we deposit Pd in a gradual manner on graphene instead of HOPG: a total of eight deposition steps were employed to get to an overall Pd thickness of ∼2.5 nm. ARXPS data were collected after each deposition.

Figure 3a shows the progressive appearance of the Pd−carbide C peak at 284.0 eV. One may question the

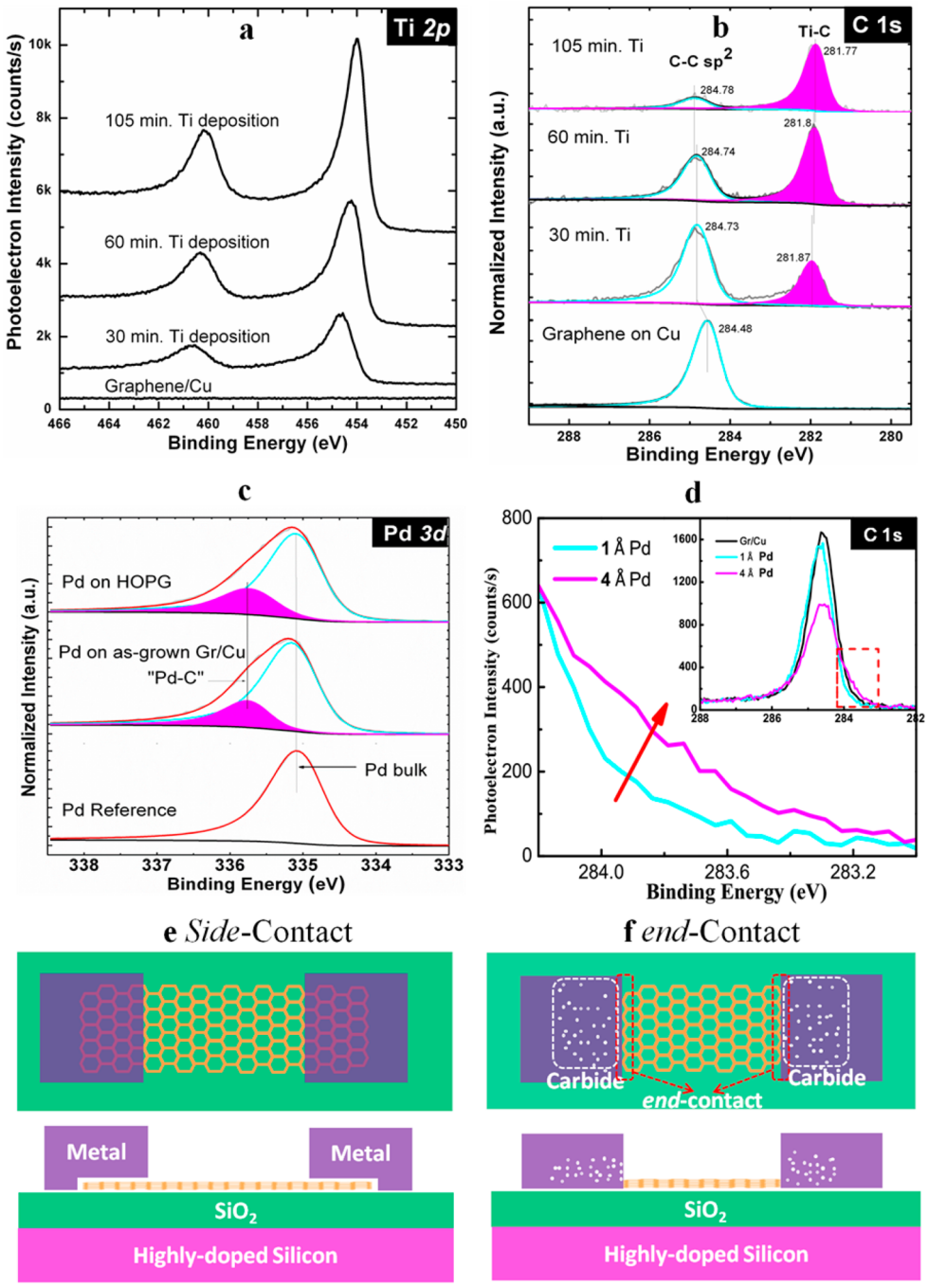

Figure 2. (a) Ti 2p and (b) C 1s XPS spectra for the 30 min (~0.6 nm), 60 min (~1.5 nm), and 105 min (~3.0 nm) deposition of Ti on as-grown Gr/Cu. (c) Pd $3d_{5/2}$ XPS spectra for the Pd deposition on as-grown Gr/Cu (~0.6 nm Pd) and HOPG (~0.8 nm Pd) and (d) C 1s XPS spectra for ~0.1 and ~0.4 nm Pd deposition on as-grown Gr/Cu. The schematic illustration of metal−graphene (e) side-contact and (f) end-contact structures. The white dots in (f) represent the carbon atoms in the metal−carbide alloy.

assignment of the 284.0 and 335.7 eV peaks to be the C peak and Pd peak in Pd−carbide; that is, can the graphene film covered by palladium without Pd−C alloy formation (as represented by Figure 1b,c) lead to the detected peaks? In other words, is it possible to observe a chemical shift 0.6 eV higher for the Pd peak and a 0.6 eV lower C peak by simply stacking Pd on the graphene sheet without any chemical reaction? We attribute these two peaks to the Pd−C alloy (*i.e.*, Pd−carbide). Angle-resolved XPS provides the convincing evidence that (i) the detected C peak is not from the interface but from the surface, and (ii) the detected Pd peak is not from the interface but from a uniform alloy also on the surface. For convenience, the peak corresponding to the carbon in graphene at ~284.6 eV is labeled "C−C"; the peak corresponding to the carbon in the Pd−carbide at ~284.0 eV is labeled "C−Pd"; the peak corresponding to the Pd in the Pd−carbide at ~335.7 eV is labeled "Pd−C", and the peak corresponding to the metallic Pd reference at 335.1 eV is labeled "Pd−Pd". The metallic Pd reference is

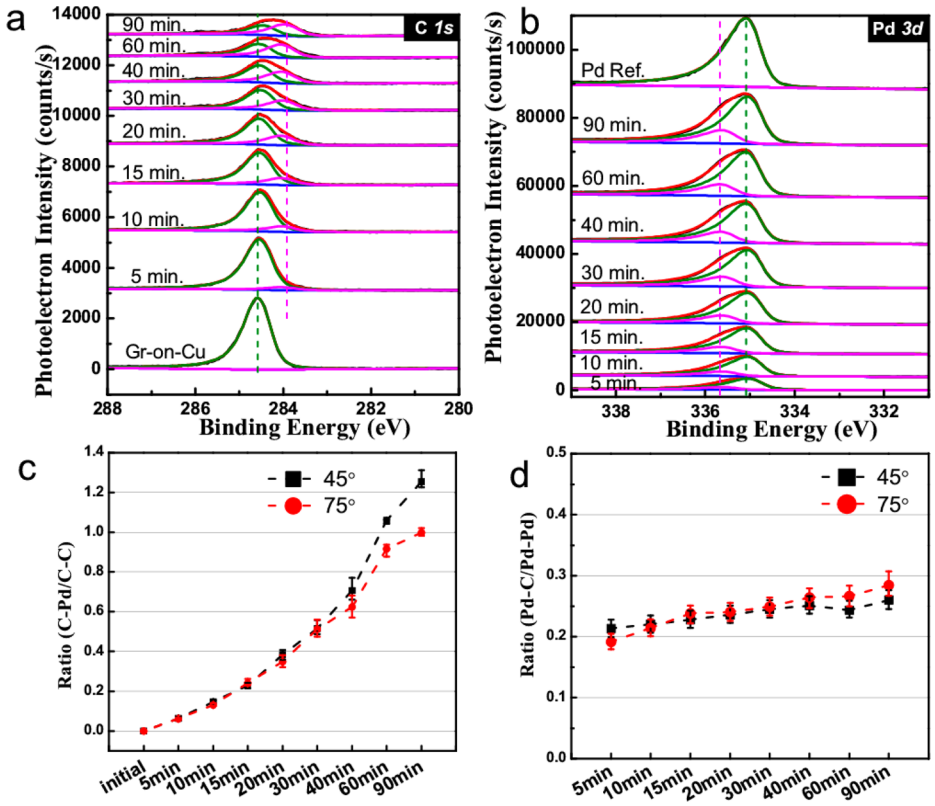

Figure 3. The 45° acquisition of (a) C 1s and (b) Pd $3d_{5/2}$ XPS spectra of the Gr/Cu sample with increasing time of Pd deposition. (c) Ratio of the C 1s peak intensity of C−Pd bonding to that of sp^2 C−C bonding, with increased Pd deposition time, from θ = 45 and 75° acquisitions. (d) Ratio of the Pd peak intensity of Pd−C bonding to that of metallic Pd, with increased Pd deposition time, from θ = 45 and 75° acquisitions.

obtained by depositing a suitable thickness (tens of nanometers) of Pd on a pure Cu surface.

First, as shown in Figure 3d, as the amount of Pd increases with thickness, the larger C−Pd/C−C ratio at a takeoff angle of θ = 45° compared to θ = 75° (see Figure 1a for the meaning of "θ") indicates that "C−Pd" is present at the surface instead of the buried interface. (In ARXPS, the θ = 45° spectra are surface-sensitive, in comparison with the θ = 75° spectra that are interface-sensitive.) In Figure 3d, the initial cycles of deposition (≤30 min) result in approximately three atomic layers of Pd. Considering island nucleation without a full metal coverage of the graphene, it is thus still meaningless to discuss the difference between "surface" and "interface" for such thin, discontinuous layers. However, with the thicker Pd deposition, the surface structures can be distinguished from the buried interface by ARXPS due to the photoelectron escape depth. Therefore, after a 2.5 nm Pd deposition (90 min in Figure 3c), ARXPS at θ = 45° shows a higher C−Pd/C−C ratio than for θ = 75°. This suggests that the detected C−Pd bonding stems from the surface structure; that is, these carbon atoms are within the deposited Pd layers.

Second, two behaviors in the spectra shown in Figure 3d suggest a Pd−C alloy of a uniform phase. (i) There is no clear difference between θ = 45 and 75° measurements within the error for all the depositions, and (ii) unlike the drastic increase of C−Pd/C−C ratio in Figure 3c, the Pd−C/Pd−Pd ratio remains almost unchanged (~0.2−0.3) for all depositions. Both phenomena are consistent with a uniform phase of the Pd−C alloy on copper (see Figure 1e), instead of at the interface (see Figure 1b,c) or at the top surface (see Figure 1d).

The XPS results show that the predominant Ti−carbide C peak with respect to the sp^2 C 1s peak indicates the reaction between the deposited Ti and the graphene, resulting in the consumption of the underlying graphene. Considering patterned graphene from a device perspective, the resulting contact geometry between Ti and graphene will therefore be primarily an end-contact, as illustrated in Figure 2f. In a relatively weaker chemical interaction with Pd, graphene can still be severely damaged by the Pd deposition. Based on the estimated high C/Pd atomic ratio in the carbide (1:5.5), graphene can also be consumed with ease under the deposition kinetics. However, normally during the device fabrication process in many laboratories, whatever types of graphene are used (*e.g.*, exfoliated graphene, epitaxial graphene on SiC, or transferred graphene from metal templates), there is always electron-beam resist residues or photoresist residues on graphene. These contaminants inevitably weaken the direct interaction between deposited metals and graphene.[49] Moreover, reactive metals favor

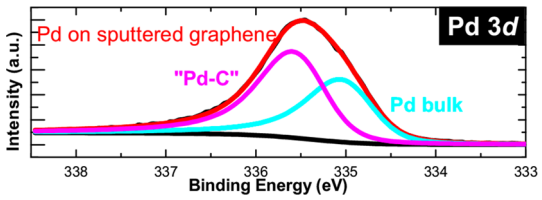

Figure 4. XPS spectrum of Pd $3d_{5/2}$ core level shift after ~0.9 nm Pd deposition on He-sputtered (reactive) CVD graphene.

oxidization and carbidization in non-UHV deposition conditions.[34,35] Therefore, the metal–graphene contact in many as-prepared devices may be a complicated combination of both end-contact and side-contact interactions. One may expect a varying percentage of end-contact configuration from device to device, depending on the metals (*e.g.*, purity, reactivity, *etc.*), the deposition conditions (*e.g.*, vacuum levels, deposition temperatures, *etc.*), the sample qualities (*e.g.*, graphene cleanness), and the post-annealing.

Palladium–Graphene Reaction. The formation of Pd–carbide originates from a strong interface chemical reaction, instead of a simple process of carbon diffusion into metals, considering that the room temperature carbon solubility in Pd is even lower than 0.1%.[46] The chemical interaction between hydrocarbons and Pd surfaces has been reported with the formation of surface Pd–carbide.[44,45] The other evidence in support of the reaction mechanism rather than the diffusion mechanism is the observation that the ratio of Pd–carbide XPS signal to the metallic Pd XPS signal is increased by depositing Pd on a defective graphene. It is known that the reactivity of graphene is effectively enhanced by making it defective. Through predeposition helium ion bombardment on a separate sample, we show that there is an increased carbon concentration in the resulting Pd–carbide.

An ion gun (model FIG-SCE 5 kV Physical Electronics, Inc.) was used to perform sputtering using helium as the source. The sputtering lasted for 2 min at a beam voltage of 1 kV, with a spot size of 4 × 4 mm. The X-ray photoelectron spectrometer and the ion gun are located in the same chamber. XPS was taken before and after He sputtering in the same region. After Pd was deposited on the sample in the metal deposition chamber and transferred to the XPS analysis chamber, the position was monitored and precisely controlled so that XPS was taken in the same sputtered spot.

After He ion sputtering the as-synthesized CVD graphene on copper foil, ~0.9 nm thick Pd was deposited. In this UHV environment, a number of defects in the graphene sheet are produced after He ion sputtering, promoting the reactivity of graphene. Therefore, *in situ* Pd deposition on the sputtered graphene sheet involves a stronger chemical reaction between Pd and graphene. The XPS data in Figure 4 show an increased Pd–C/Pd–Pd ratio (~1.5), compared with the Pd deposition on as-synthesized graphene (~0.25, as shown in Figure 2c and 3b,d). This result is strong evidence that the Pd–graphene chemical reaction is dependent on the reactivity of the graphene.

CONCLUSION

In summary, *in situ* XPS characterization of electron-beam-deposited Pd and Ti on as-synthesized graphene on copper in a UHV environment provides unambiguous evidence that the sp^2-bonded planar structure of graphene is disrupted by the wetting metal–graphene chemical interaction. The end-contact configuration is formed between metals and the nonreacted graphene. To generalize the impact of this work, we suspect that the broadly adopted metal–graphene side-contact model conveys physically misleading information. When wetting metals such as Pd and Ti are intended to be deposited on graphene, two likely results would be gained. The first possible outcome is the strong chemical interaction and the resulting metal–carbide; that is, graphene is consumed. The second possible outcome is the oxidization and carbidization of the deposited metal by the oxygen- or carbon-bearing contaminants in the chamber or on the graphene, resulting in metal–oxide– or metal–carbide–graphene contact. Basically, the pure wetting metal–graphene interface in side-contact geometry is not expected to occur as a result of the reactive metal deposition process. Efforts on the fabrication of metal–graphene end-contact[29,50] have been devoted with reduced contact resistances demonstrated.[13,51] Recently, a study of metal–graphene end-contact has been reported.[52] In contrast to these reports, this work provides experimental validation of the spontaneous formation of end-contacts when wetting metals are deposited on clean graphene films under well-controlled vacuum conditions.

EXPERIMENTAL METHODOLOGIES

Graphene Synthesis, Metal Deposition, and XPS Characterization. The CVD graphene samples employed in this work were grown on 25 μm thick Cu foils (Alfa Aesar, 99.8% purity) in a halogen lamp-based quartz tube furnace at a growth temperature of 1035 °C with 5 sccm of H_2 and 7 sccm of CH_4 flowing during growth with a total pressure of 400 Torr.[36,53] Graphene grown by this method has a grain size of 10–20 μm as determined by scanning electron microscope imaging. The samples were then loaded into the cluster XPS analysis chamber, where analysis was carried out using a monochromatic Al Kα X-ray source.[39] An analyzer acceptance angle of 8°, a takeoff angle of 45° (by default) or 75° (angle between the detector and the sample surface in ARXPS study), and pass energy of 15 eV were employed in this study. Pd and Ti were deposited on the as-synthesized graphene with an electron-beam evaporation source in a UHV chamber connected to the analysis chamber and were outgassed for 2 h prior to deposition to avoid any metal oxide remnants at the surface. The metal Pd and Ti were

deposited at $\sim 1 \times 10^{-8}$ mbar (base pressure $\sim 1 \times 10^{-9}$ mbar) with the sample at nominally room temperature. XPS analysis was carried out after each deposition.

Conflict of Interest: The authors declare no competing financial interest.

Acknowledgment. This work is funded by the Semiconductor Research Corporation NRI SWAN center. K.C. is partially supported by Nano·Material Technology Development Program through the National Research Foundation of Korea (NRF) funded by the Ministry of Science, ICT and Future Planning (2012M3A7B4049888). D. Hinojos is acknowledged for growing graphene in Prof. R. M. Wallace's lab.

Supporting Information Available: XPS evidence for the absence of residual oxygen on clean HOPG; details about the electron-beam deposition of palladium and titanium. This material is available free of charge *via* the Internet at http://pubs.acs.org.

REFERENCES AND NOTES

1. Novoselov, K. S.; Geim, A. K.; Morozov, S. V.; Jiang, D.; Zhang, Y.; Dubonos, S. V.; Grigorieva, I. V.; Firsov, A. A. Electric Field Effect in Atomically Thin Carbon Films. *Science* **2004**, *306*, 666–669.
2. Giovannetti, G.; Khomyakov, P. A.; Brocks, G.; Karpan, V. M.; van den Brink, J.; Kelly, P. J. Doping Graphene with Metal Contacts. *Phys. Rev. Lett.* **2008**, *101*, 026803.
3. Khomyakov, P. A.; Giovannetti, G.; Rusu, P. C.; Brocks, G.; van den Brink, J.; Kelly, P. J. First-Principles Study of the Interaction and Charge Transfer between Graphene and Metals. *Phys. Rev. B* **2009**, *79*, 195425.
4. Gong, C.; Lee, G.; Shan, B.; Vogel, E. M.; Wallace, R. M.; Cho, K. First-Principles Study of Metal–Graphene Interfaces. *J. Appl. Phys.* **2010**, *108*, 123711.
5. Gong, C.; Hinojos, D.; Wang, W. C.; Nijem, N.; Shan, B.; Wallace, R. M.; Cho, K. J.; Chabal, Y. J. Metal–Graphene–Metal Sandwich Contacts for Enhanced Interface Bonding and Work Function Control. *ACS Nano* **2012**, *6*, 5381–5387.
6. Barraza-Lopez, S.; Vanevic, M.; Kindermann, M.; Chou, M. Y. Effects of Metallic Contacts on Electron Transport through Graphene. *Phys. Rev. Lett.* **2010**, *104*, 076807.
7. Maassen, J.; Ji, W.; Guo, H. First Principles Study of Electronic Transport through a Cu(111)|Graphene Junction. *Appl. Phys. Lett.* **2010**, *97*, 142105.
8. Tworzydlo, J.; Trauzettel, B.; Titov, M.; Rycerz, A.; Beenakker, C. W. J. Sub-Poissonian Shot Noise in Graphene. *Phys. Rev. Lett.* **2006**, *96*, 246802.
9. Titov, M.; Beenakker, C. W. J. Josephson Effect in Ballistic Graphene. *Phys. Rev. B* **2006**, *74*, 041401(R).
10. Fu, L.; Kane, C. L. Semiconducting Proximity Effect and Majorana Fermions at the Surface of a Topological Insulator. *Phys. Rev. Lett.* **2008**, *100*, 096407.
11. Poumirol, J. M.; Cresti, A.; Roche, S.; Escoffier, W.; Goiran, M.; Wang, X. R.; Li, X. L.; Dai, H. J.; Raquet, B. Edge Magnetotransport Fingerprints in Disordered Graphene Nanoribbons. *Phys. Rev. B* **2010**, *82*, 041413.
12. Xia, F. N.; Perebeinos, V.; Lin, Y. M.; Wu, Y. Q.; Avouris, P. The Origins and Limits of Metal–Graphene Junction Resistance. *Nat. Nanotechnol.* **2011**, *6*, 179–184.
13. Robinson, J. A.; LaBella, M.; Zhu, M.; Hollander, M.; Kasarda, R.; Hughes, Z.; Trumbull, K.; Cavalero, R.; Snyder, D. Contacting Graphene. *Appl. Phys. Lett.* **2011**, *98*, 053103.
14. Dicarlo, L.; Williams, J. R.; Zhang, Y.; McClure, D. T.; Marcus, C. M. Shot Noise in Graphene. *Phys. Rev. Lett.* **2008**, *110*, 156801.
15. Nouchi, R.; Shiraishi, M.; Suzuki, Y. Transfer Characteristics in Graphene Field-Effect Transistors with Co Contacts. *Appl. Phys. Lett.* **2008**, *93*, 152104.
16. Venugopal, A.; Colombo, L.; Vogel, E. M. Contact Resistance in Few and Multilayer Graphene Devices. *Appl. Phys. Lett.* **2010**, *96*, 013512.
17. Nagashio, K.; Nishimura, T.; Kita, K.; Toriumi, A. Contact Resistivity and Current Flow Path at Metal/Graphene Contact. *Appl. Phys. Lett.* **2010**, *97*, 143514.
18. Nagashio, K.; Toriumi, A. Density-of-States Limited Contact Resistance in Graphene Field-Effect Transistors. *Jpn. J. Appl. Phys.* **2011**, *50*, 070108.
19. Lahiri, J.; Batzill, M. Graphene Destruction by Metal–Carbide Formation: An Approach for Patterning of Metal-Supported Graphene. *Appl. Phys. Lett.* **2010**, *97*, 023102.
20. Boukhvalov, D. W.; Katsnelson, M. I. Destruction of Graphene by Metal Adatoms. *Appl. Phys. Lett.* **2009**, *95*, 023109.
21. Zhang, Y.; Ichihashi, T.; Landree, E.; Nihey, F.; Iijima, S. Heterostructures of Single-Walled Carbon Nanotubes and Carbide Nanorods. *Science* **1999**, *285*, 1719–1722.
22. Leonard, F.; Tersoff, J. Role of Fermi-Level Pinning in Nanotube Schottky Diodes. *Phys. Rev. Lett.* **2000**, *84*, 4693–4696.
23. Ramasse, Q. M.; Zan, R.; Bangert, U.; Boukhvalov, D. W.; Son, Y. W.; Novoselov, K. S. Direct Experimental Evidence of Metal-Mediated Etching of Suspended Graphene. *ACS Nano* **2012**, *6*, 4063–4071.
24. Lee, E. J. H.; Balasubramanian, K.; Weitz, R. T.; Burghard, M.; Kern, K. Contact and Edge Effects in Graphene Devices. *Nat. Nanotechnol.* **2008**, *3*, 486–490.
25. Nagashio, K.; Moriyama, T.; Ifuku, R.; Yamashita, T.; Nishimura, T.; Toriumi, A. Is Graphene Contacting with Metal Still Graphene? *IEEE International Electron Devices Meeting* **2011**, 10.1109/IEDM.2011.6131475.
26. Lin, Y. F.; Wang, S. T.; Pao, C. C.; Li, Y. C.; Lai, C. C.; Lin, C. K.; Hsu, S. Y.; Jian, W. B. Probing into the Metal–Graphene Interface by Electron Transport Measurements. *Appl. Phys. Lett.* **2013**, *102*, 033107.
27. Huard, B.; Stander, N.; Sulpizio, J. A.; Goldhaber-Gordon, D. Evidence of the Role of Contacts on the Observed Electron–Hole Asymmetry in Graphene. *Phys. Rev. B* **2008**, *78*, 121402.
28. Ran, Q. S.; Gao, M. Z.; Guan, X. M.; Wang, Y.; Yu, Z. P. First-Principles Investigation on Bonding Formation and Electronic Structure of Metal–Graphene Contacts. *Appl. Phys. Lett.* **2009**, *94*, 103511.
29. Matsuda, Y.; Deng, W. Q.; Goddard, W. A. Contact Resistance for "End-Contacted" Metal–Graphene and Metal–Nanotube Interfaces from Quantum Mechanics. *J. Phys. Chem. C* **2010**, *114*, 17845–17850.
30. Matsuda, Y.; Deng, W. Q.; Goddard, W. A. Contact Resistance Properties between Nanotubes and Various Metals from Quantum Mechanics. *J. Phys. Chem. C* **2007**, *111*, 11113–11116.
31. Mann, D.; Javey, A.; Kong, J.; Wang, Q.; Dai, H. J. Ballistic Transport in Metallic Nanotubes with Reliable Pd Ohmic Contacts. *Nano Lett.* **2003**, *3*, 1541–1544.
32. Wang, Q. J.; Che, J. G. Origins of Distinctly Different Behaviors of Pd and Pt Contacts on Graphene. *Phys. Rev. Lett.* **2009**, *103*, 066802.
33. Javey, A.; Guo, J.; Wang, Q.; Lundstrom, M.; Dai, H. J. Ballistic Carbon Nanotube Field-Effect Transistors. *Nature* **2003**, *424*, 654–657.
34. Pirkle, A.; Colombo, L.; Wallace, R. M. *In Situ* Studies of Al_2O_3 and HfO_2 Dielectrics on Graphite. *Appl. Phys. Lett.* **2009**, *95*, 133106.
35. Pirkle, A.; Chabal, Y. J.; Colombo, L.; Wallace, R. M. *In Situ* Studies of High-κ Dielectrics for Graphene-Based Devices. *ECS Trans.* **2009**, *19*, 215–224.
36. Pirkle, A.; Chan, J.; Venugopal, A.; Hinojos, D.; Magnuson, C. W.; McDonnell, S.; Colombo, L.; Vogel, E. M.; Ruoff, R. S.; Wallace, R. M. The Effect of Chemical Residues on the Physical and Electrical Properties of Chemical Vapor Deposited Graphene Transferred to SiO_2. *Appl. Phys. Lett.* **2011**, *99*, 122108.
37. Gong, C.; Floresca, H. C.; Hinojos, D.; McDonnell, S.; Qin, X.; Hao, Y.; Jandhyala, S.; Mordi, G.; Kim, J.; Colombo, L.; *et al.* Rapid Selective Etching of PMMA Residues from Transferred Graphene by Carbon Dioxide. *J. Phys. Chem. C* **2013**, *117*, 23000–23008.
38. Lin, Y. C.; Lu, C. C.; Yeh, C. H.; Jin, C. H.; Suenaga, K.; Chiu, P. W. Graphene Annealing: How Clean Can It Be? *Nano Lett.* **2012**, *12*, 414–419.

39. Wallace, R. M. *In Situ* Studies of Interfacial Bonding of High-k Dielectrics for CMOS beyond 22nm. *ECS Trans.* **2008**, *16*, 255–271.
40. Chan, J.; Venugopal, A.; Pirkle, A.; McDonnell, S.; Hinojos, D.; Magnuson, C. W.; Ruoff, R. S.; Colombo, L.; Wallace, R. M.; Vogel, E. M. Reducing Extrinsic Performance-Limiting Factors in Graphene Grown by Chemical Vapor Deposition. *ACS Nano* **2012**, *6*, 3224–3229.
41. Gong, C.; Huang, C.; Miller, J.; Cheng, L.; Hao, Y.; Cobden, D.; Kim, J.; Ruoff, R. S.; Wallace, R. M.; Cho, K.; *et al.* Metal Contacts on Physical Vapor Deposited Monolayer MoS_2. *ACS Nano* **2013**, 10.1021/nn4052138.
42. Galuska, A. A.; Uht, J. C.; Marquez, N. Reactive and Nonreactive Ion Mixing of Ti Films on Carbon Substrates. *J. Vac. Sci. Technol., A* **1988**, *6*, 110–122.
43. Seriani, N.; Mittendorfer, F.; Kresse, G. Carbon in Palladium Catalysts: A Metastable Carbide. *J. Chem. Phys.* **2010**, *132*, 024711.
44. Teschner, D.; Borsodi, J.; Wootsch, A.; Revay, Z.; Havecker, M.; Knop-Gericke, A.; Jackson, S. D.; Schlogl, R. The Roles of Subsurface Carbon and Hydrogen in Palladium-Catalyzed Alkyne Hydrogenation. *Science* **2008**, *320*, 86–89.
45. Teschner, D.; Revay, Z.; Borsodi, J.; Havecker, M.; Knop-Gericke, A.; Schlogl, R.; Milroy, D.; Jackson, S. D.; Torres, D.; Sautet, P. Understanding Palladium Hydrogenation Catalysts: When the Nature of the Reactive Molecule Controls the Nature of the Catalyst Active Phase. *Angew. Chem., Int. Ed.* **2008**, *47*, 9274–9278.
46. Massalski, T. B.; Okamoto, H.; Subramanian, P. R.; Kacprzak, L. *Binary Alloy Phase Diagrams*; ASM International: Materials Park, OH, 1990; Vol. 1.
47. Jirka, I.; Plsek, J.; Vondracek, M.; Sutara, F.; Matolin, V.; Chab, V.; Prince, K. C. Interaction of Ethylene with Palladium Clusters Supported on Oxidised Tungsten Foil. *Surf. Sci.* **2007**, *601*, 3114–3124.
48. Teschner, D.; Wild, U.; Schlogl, R.; Paal, Z. Surface State and Composition of a Disperse Pd Catalyst after Its Exposure to Ethylene. *J. Phys. Chem. B* **2005**, *109*, 20516–20521.
49. Watanabe, E.; Conwill, A.; Tsuya, D.; Koide, Y. Low Contact Resistance Metals for Graphene Based Devices. *Diamond Relat. Mater.* **2012**, *24*, 171–174.
50. Gong, C.; Lee, G.; Wang, W.; Shan, B.; Vogel, E. M.; Wallace, R. M.; Cho, K. First-Principles and Quantum Transport Studies of Metal−Graphene End Contacts. *MRS Online Proc. Libr.* **2010**, *1259*, S14–35.
51. Smith, J. T.; Franklin, A. D.; Farmer, D. B.; Dimitrakopoulos, C. D. Reducing Contact Resistance in Graphene Devices through Contact Area Patterning. *ACS Nano* **2013**, *7*, 3661–3667.
52. Wang, L.; Meric, I.; Huang, P. Y.; Gao, Q.; Gao, Y.; Tran, H.; Taniguchi, T.; Watanabe, K.; Campos, L. M.; Muller, D. A.; *et al.* One-Dimensional Electrical Contact to a Two-Dimensional Material. *Science* **2013**, *342*, 614–617.
53. Li, X. S.; Cai, W. W.; An, J. H.; Kim, S.; Nah, J.; Yang, D. X.; Piner, R.; Velamakanni, A.; Jung, I.; Tutuc, E.; *et al.* Large-Area Synthesis of High-Quality and Uniform Graphene Films on Copper Foils. *Science* **2009**, *324*, 1312–1314.